Indian Journal of Pure & Applied Physics
Vol. 57, March 2019, pp. 166-174

Optimizations of preparative parameters in potentiodynamic synthesis of cobalt oxide thin films: Capacitive approach

S V Khavale & B J Lokhande*

School of Physical Sciences, Solapur University, Solapur 413 255, India

Received 14 February 2017; accepted 24 October 2018

The present article reports synthesis of Co_3O_4 thin films by facile potentiodynamic-electrodeposition technique using variations in the preparative parameters such as ingredient, solution concentration and deposition time. The prepared samples were analysed using XRD, FE-SEM, TEM, cyclic voltammetry, chronopotentiometry and electrochemical impedance spectroscopy. Crystallographic study shows polycrystalline face centered cubic spinel structure of the deposit. Cyclic voltammogram reveals pseudocapacitive behavior. The calculated highest value of specific capacitance at the scan rate 5 mV/s was 237.68 F/gin 1 M KOH, within the potential window -0.92 to 0.45 V versus Ag/AgCl. The calculated maximum value of specific energy, specific power and columbic efficiency from chronopotentiometry were 4.91 Wh/kg, 28.69 kW/kg and 94.78%, respectively. The internal resistance observed using electrochemical impedance spectroscopy was~ 3.55 Ω.

Keywords: Potentiodynamic electrodeposition, Cobalt oxide, Supercapacitor electrode, Cyclic voltammogram, Impedance

1 Introduction

Currently energy production and storage are the most imperative issues for the economic and industrial development. The most promising source of clean energy is sunlight acting in a sustainable way. Since solar energy is one of the sustainable and clean source of energy, tremendous amount of work is going on now-a-days to convert solar energy into chemical energy by generation of hydrogen as a fuel[1,2] and solar energy into electrical energy photovoltaic devices[3,4]. On the other hand, the energy storage devices, such as rechargeable small-sized ion batteries[5,6] have also been preferred. Among several kinds of energy storage devices, electrochemical capacitors/supercapacitors (SCs) became noticeable because of their high energy density, high energy efficiency and long charge-discharge cycle life[7]. The SCs are categorized into two types based on charge storage mechanism, one is electrochemical double layer capacitors (EDLCs), *i.e.*, non-faradaic and the second is pseudocapacitors or faradaic capacitors[8,9]. SCs possess higher power density and more rapid charge-discharge rate as compared to conventional batteries[10,11]. Nevertheless, a lower amount of energy density and life-times of SCs, in contrast with rechargeable batteries, are two key challenges for scientists. Researchers are trying to increase the energy, power density and stability of the pristine materials. To achieve these targets, researchers have turned their attention in the past few years towards different morphology dependent materials like transition metal oxides (TMOs) such as ruthenium (IV) oxide[12], manganese dioxide[13-15], cobalt oxide/ hydroxide[16-19], nickel(II)oxide/ hydroxide[20-22], Fe_3O_4[23] etc. as electrode in supercapacitor. Among these metal oxides, cobalt oxide based electrode showed different morphologies with improvement in the supercapacitive performance and posse's 3500 F/g maximum value of theoretical capacitance[24-26]. Recent study reports Co_3O_4 nanostructures with various morphologies including nano-particles[27], nanowires[28,29], nanotubes[30] and nano-sheets[31] which have been successfully synthesized by changing preparative parameters and methods in order to improve the super capacitive properties.

Intention of present study is to check the improvement in the capacitive performances of pristine cobalt oxide thin film electrodes by varying different cobalt ingredients, molar concentrations of the optimized ingredient solution and deposition time of the electrode.

2 Experimental Details

2.1 Materials and methods

All the chemicals used during the synthesis are of analytical grade, purchased from Sigma Aldrich chemicals and are used without any further purification. Template-free, binder-less cobalt

*Corresponding author (E-mail: bjlokhande@yahoo.com)

hydroxide layers were potentiodymically electrodeposited on well cleaned stainless steel (SS) substrates (no. 304, 1×5 cm^2) using conventional three-electrode cell configuration. Here the platinum was used as a counter electrode and Ag/AgCl was used as a reference electrode. Computer controlled potentiostat (CHI 600 D Electrochemical Analyzer/workstation, CH instruments, USA) was used to carry the potentiodynamic electrodeposition. Prior to the deposition,0.1M solutions were prepared in double distilled water using different ingredients like cobaltous chloride hexa-hydrate ($CoCl_2.6H_2O$), cobaltous nitratehexa-hydrate ($Co(NO_3)_2.6H_2O$), cobaltous acetatetetra-hydrate ($C_4H_6CoO_4.4H_2O$). The SS substrates were etched prior to each experiment using a diluted hydrochloric acid (Merck, 60%) for 1 min and finally washed and ultrasonically cleaned with double distilled water. During the deposition, deposition potential window, deposition scan rate and deposition time was maintained as -1.0 V to -0.1 V, 100 mV/s and 30 min, respectively. Further, the samples were deposited for different molar concentrations and deposition times. The deposited samples were annealed at 300 °C for 1.5 h for complete conversion of cobalt hydroxide to cobalt oxide (Co_3O_4).

The obtained Co_3O_4 samples were nomenclature as; for ingredients: cobalt chloride- A, cobalt nitrate-B and cobalt acetate- C, for molar concentration variation: M_1:0.05M, M_2: 0.1M, M_3:0.15M, M_4:0.2M, M_5:0.25M, M_6:0.3M and for deposition time variation D_1: 20 min, D_2: 30 min, D_3: 40 min, D_4: 50 min and D_5: 60 min, respectively.

2.2 Characterizations

X-ray diffraction analysis was carried out using (Rigaku D/max 2550 Vb^+/PC 18 kW with Cu k$\alpha\lambda$=0.15405 nm) diffractometer by varying diffraction angle 2θ within the range of 20°-80°. Surface morphological analysis was performed by using filed emission-scanning electron microscope (FE-SEM; MIRA3, TESCAN). Weight of the deposited materials was measured by weight difference method using ultrasensitive, high accuracy analytical microbalance (Tapson's Model6-100 TS). Electrochemical supercapacitive behavior of the prepared electrodes was carried out using computer controlled potentiostat (CHI600D electrochemical analyzer/workstation, CH instruments USA) with standard three electrodes cell configuration. Here the prepared Co_3O_4 electrodes were used as the working electrodes, platinum as a counter electrode and saturated Ag/AgCl as a reference electrode. The cyclic voltammetry (CV) was carried out within the potential window of -0.92 to 0.45 V in 1 M KOH at the scan rate of 5 mV/s for each electrode. Charge-discharge behavior of the prepared electrodes was studied at different current densities using chronopotentiometry. Multi frequency impedance measurements were made in the frequency range 1 mHz to 1 MHz using AC signal with open circuit potential (OCP) at -0.38 V applied with 5 mV amplitude. Electrochemical impedance spectroscopy (EIS) data was fitted with standard data to search an equivalent circuit and parameters using ZsimpWin software.

2.3 Electrochemical measurements

From the CV curves, *S*C (Specific capacitance) values were calculated using the following equations[32]:

$$C = \frac{\int Idt}{dv/dt} \quad \ldots (1)$$

$$SC = C/w \quad \ldots (2)$$

where, $\int Idt$ is the area under curve, $\frac{dv}{dt}$ is the voltage scan rate, C is the capacitance, w is the weight of the active material dipped in electrolyte.

The specific energy (SE), specific power (SP) and columbic efficiency η (%) were estimated using the following relations.

$$SE = (V \times I_d \times t_d)/w \quad \ldots (3)$$

$$SP = (V \times I_d)/w \quad \ldots (4)$$

$$\eta = (t_d \times 100)/w \quad \ldots (5)$$

Where, t_c and t_d represent the time of charge and discharge, I is the current density and V is the applied voltage. w is the active weight of the sample dipped in the electrolyte.

3 Results and Discussion

3.1 Film formation mechanism

The cobalt oxide thin films were potentiodynamically electrodeposited from the three different ingredients; cobalt chloride (A), cobalt nitrate (B) and cobalt acetate (C) onto the SS substrate. During electrodeposition, the cobalt ions or complexes were hydrolyzed by aqueous solution to form the hydroxide deposits on the working electrode. After annealing at 300 °C for 1.5 h, the CoO(OH) was converted into Co_3O_4.

3.2 Film thickness

Thickness of different molar samples were calculated by gravimetric weight difference method using the relation $t=m/(\rho \times A)$; where, m is the active mass in milligram, A is the active area (cm^2) and ρ is the density of the deposited material which is assumed to be the same as that of the bulk material (ρ = 6.11 g/cm^3 for Co_3O_4). Figure 1 shows the variation of film thickness with solution concentration (M). From the figure it was observed that with increase in solution concentration, film thickness goes on increasing and it finally becomes stable beyond M_6. The rate of film thickness was not found linear with solution concentration. The stable value of film thickness was observed at higher concentration because of pilling out of film due to the increase of tensile stress that causes delamination when film becomes thick[33,34].

3.3 Structural analysis

The XRD patterns were studied to get crystallographic information, orientation of the planes for all the prepared samples. Figure 2(a-c) shows XRD patterns of the samples prepared by using different cobalt ingredients (A, B and C), different molar concentration (M_1, M_2, M_4 and M_6) and different deposition time interval (D_1, D_2, D_3 and D_5), respectively. Compared with the standard data (JCPDS, Card No. 80-1545), characteristic peaks appearing at 2θ=30.9°, 36.4°, 44.3°, 48.5°, 55°, 58.6°, 67.8°, 68.9°, 77.4° corresponding to the crystal faces (220), (311), (400), (331), (422) (511), (440),(442) and (622), respectively, confirms the face centered cubic crystal structure of Co_3O_4 electrodes. The peaks marked by asterisk belong to stainless steel substrate. It was observed that all the diffraction peaks of Co_3O_4 are broad and the intensity of certain peaks is comparatively weak, which indicate that the obtained material is poorly crystallized[35]. The similar trend was

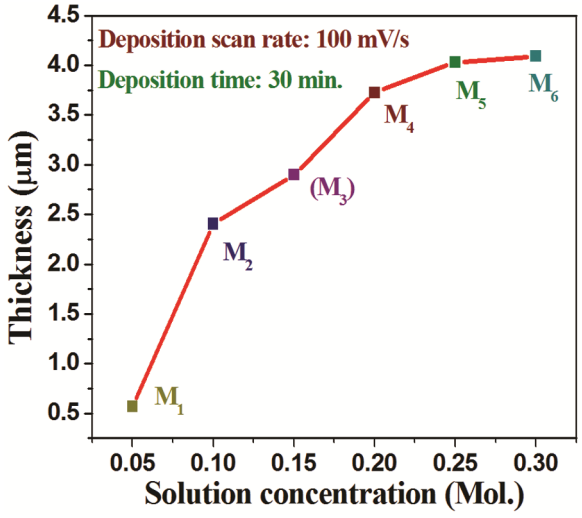

Fig. 1 — Variation of film thickness (μm) with solution concentrations (mol.) of Co_3O_4.

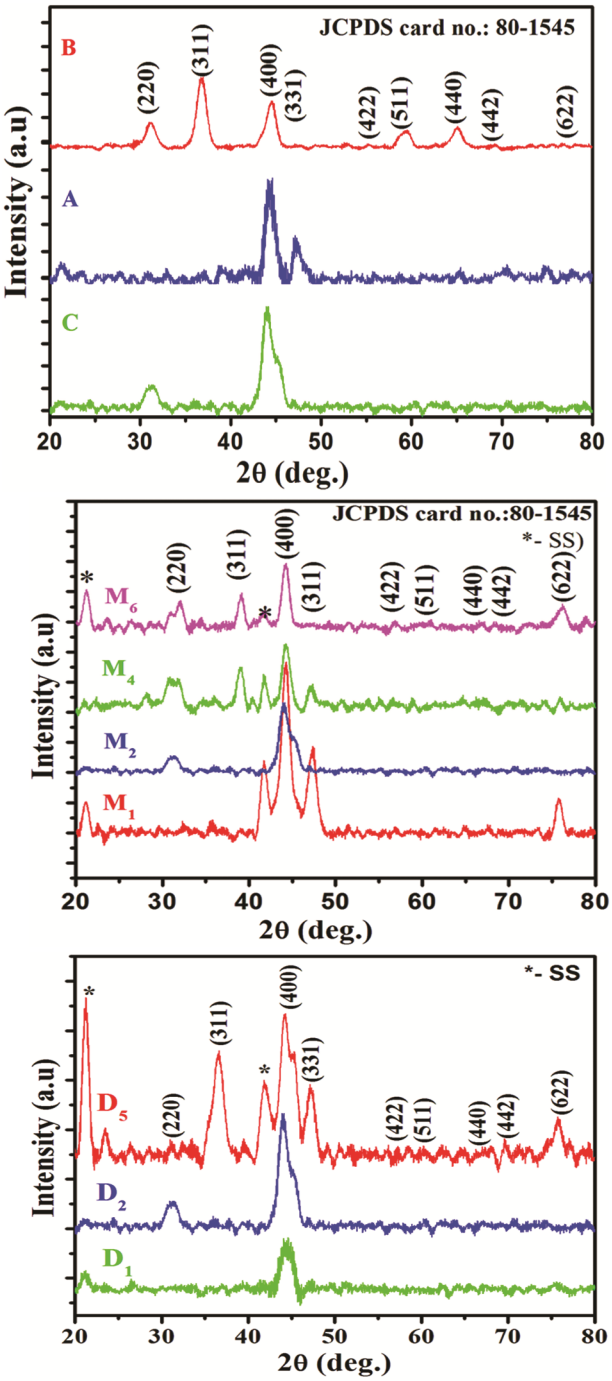

Fig. 2 — (a) XRD pattern of Co_3O_4 samples A, B and C prepared using different cobalt ingredients and (b) XRD pattern of Co_3O_4 samples M_1, M_2, M_4 and M_6 prepared using different solution concentration.

observed for the different molar concentration and also for samples deposited at different time intervals.

3.4 Morphological evolution

The morphological evolution of all the prepared samples were observed using FE-SEM images. Figure 3 (A_1-A_2, B_1–B_2 and C_1-C_2) shows the FE-SEM images of cobalt oxide samples, A, B and C, respectively. The micrograph obtained from sample A (Fig. 3 (A_1-A_2)) shows uniformly distributed granular type of morphology. Inset of figure shows magnified view of the sample clearly indicate porous nature. Similar type of morphology was observed earlier for cobalt oxide prepared by SILAR, which was feasible for supercapacitor application, as it may offer increased surface area[36,37]. The sample B shows interconnected nanoflake type of morphology, whereas the sample C shows randomly distributed nanoflake like morphology, which was consistent with the previous results, obtained using electrodeposition technique[39]. These variations in the morphology of the samples A, B and C may be attributed due to the influence of the over-potential of the anions Cl^-, $NO_3^-$and CH_3COO^- present in the precursors[20,39,40].

Figure 4 (a-d) is the typical FE-SEM images of samples for varied concentration M_2 (0.1M) and sample M_6 (0.3M). The FE-SEM micrograph images (Fig. 4 (a,b)) of sample M_2 clearly shows agglomeration of grains type morphology. While, for sample M_6 the micrograph images (Fig. 4 (c-d)) shows highly agglomerated granular type of morphology. It may concluded that, initially grown nano-grains may have increased their particle size for further deposition and particles come close to each other with increase in solution concentration.

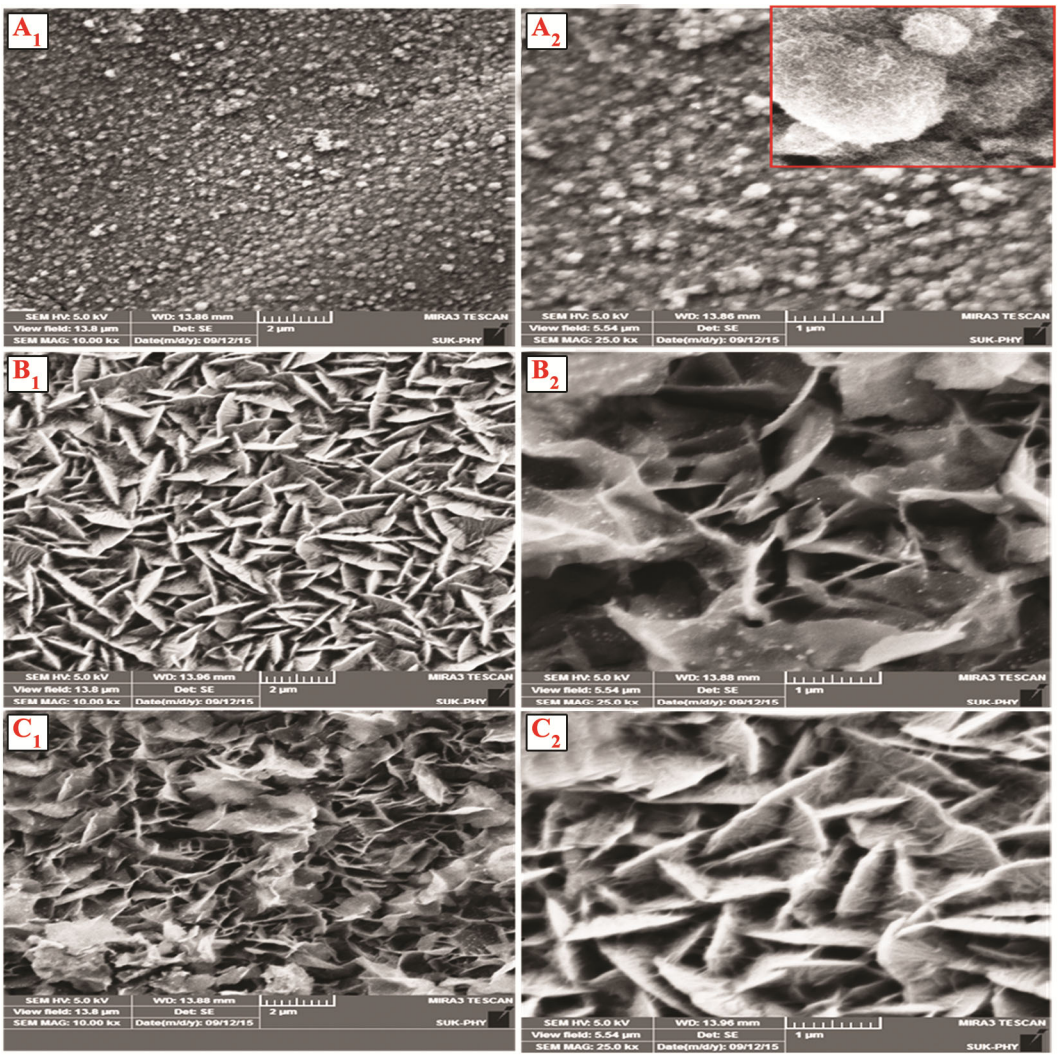

Fig. 3 — FE-SEM images of Co_3O_4 of different ingredients A, B and C at various magnifications. Inset of the figure shows magnified view.

Figure 5 shows FE-SEM images of typical D_2 (30 min) and D_5 (60 min) Co_3O_4 samples. It was observed that morphology of sample D_2 shows structural homogeneity and uniformity, which consists of fully covered-agglomerated granular particles. However as the deposition time was increased to D_5, agglomeration

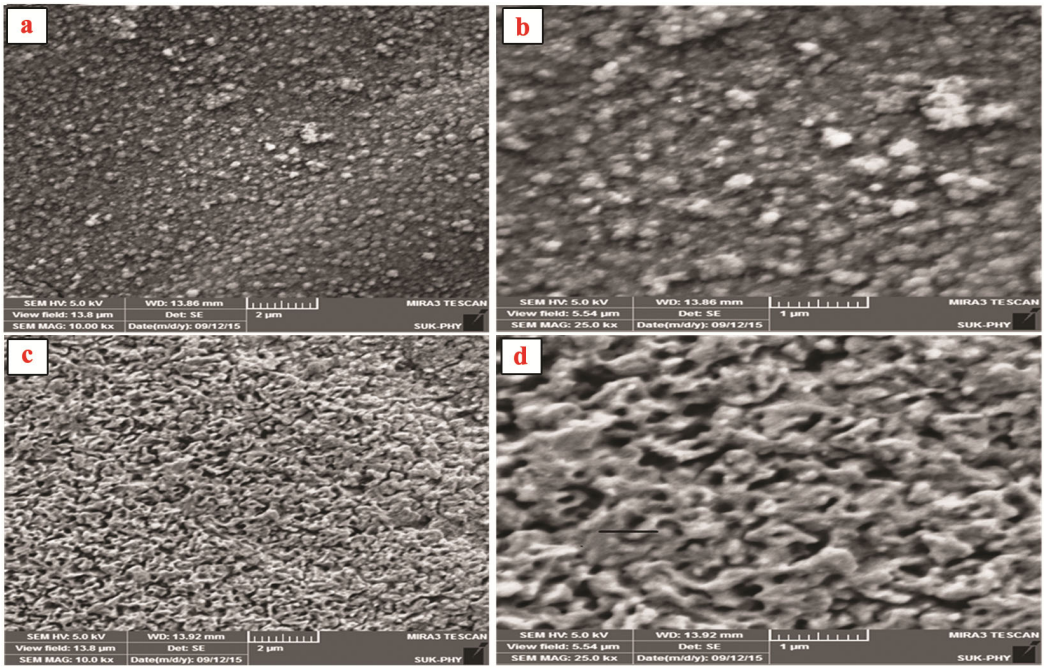

Fig. 4 — FE-SEM images of Co_3O_4 prepared using cobalt chloride as a ingredient, sample M_2 (a and b) and sample M_6 (c and d) at 10000 and 25000 magnifications.

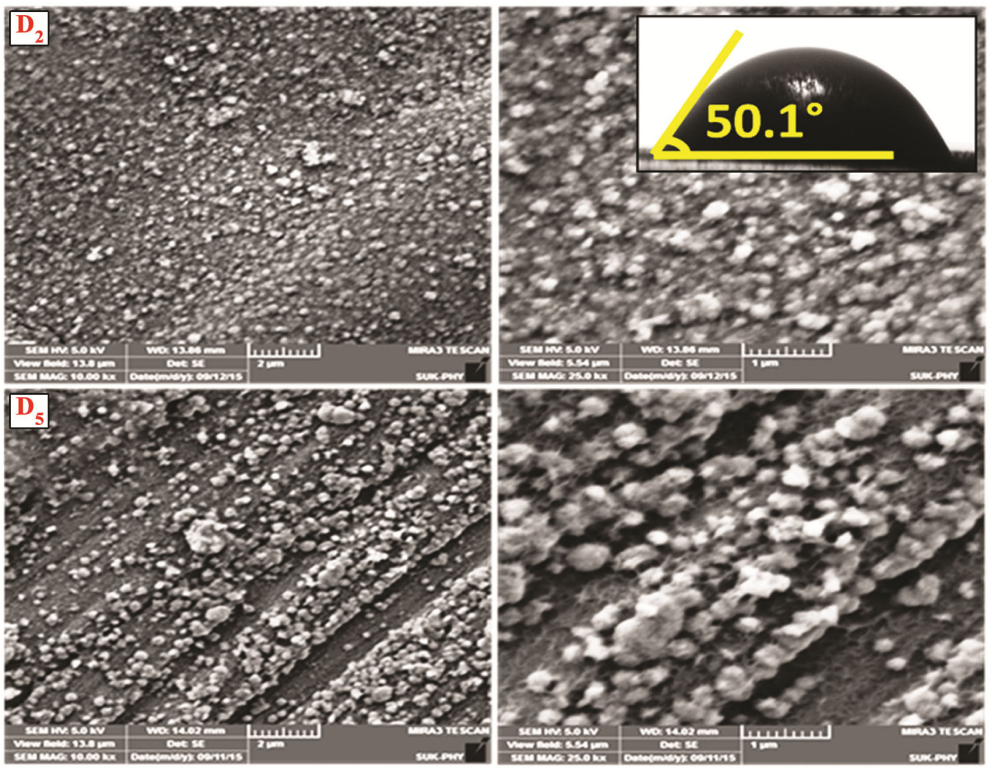

Fig. 5 — FE-SEM images of Co_3O_4 of sample M_2 carried for different deposition times. Inset of Figure shows wettability of the sample.

of the granular particles resulted into the discontinuous distribution of larger grains, which may decrease the active surface area of the electrodes.

Behavior of the liquid with the sample plays prominent role in supercapacitor performance. So wettability test was carried out for sample D_2. If the wettability is high, contact angle (θ) will be small and the surface is hydrophilic. If the wettability is low, contact angle (θ) will be large and the surface is hydrophobic. Inset of Fig. 5 depicts the contact angle measurement. Measured contact angle was about 50.1° clearly indicating hydrophilic nature of the deposit. It was earlier reported that hydrophilic surface of the electrode is an essential factor for better performance of electrochemical supercapacitor[41].

3.5 TEM analysis

Further, micro-structural analysis of typical cobalt oxide (Co_3O_4) thin film sample (D_2) was investigated using the TEM image. TEM analysis (Fig. 6) reveals that material shows granular agglomerated microstructure with porous nature of the particles. The obtained average value of particle size was around 100 nm.

3.6 Electrochemical studies

3.6.1 Cyclic voltammetry

Cyclic voltammograms were carried to observe the electrochemical performance of all the prepared samples. Figure 7 (a) shows the typical CVs of the cobalt oxide electrodes A, B and C carried at scan rate 5 mV/s in 1 M KOH within the potential window - 0.92 to 0.45 V. All CVs show psuedocapacitive behavior. Two noticeable pairs of redox peaks are observed in the CV which corresponded to the conversion between different cobalt oxidation states according to the following reactions.

$$Co_3O_4 + H_2O + OH^- \rightleftharpoons 3\ CoOOH + e^-$$

$$CoOOH + OH^- \rightleftharpoons CoO_2 + H_2O + e^-$$

The first reaction reflects the conversion between Co(II) to Co(III) for the first redox couple. The second reaction reflects the conversion between Co(III) to Co(IV) for the second redox couple[42]. These redox couples confirm the pseudocapacitive nature of the prepared electrode. Here electrode (A) obtained for chloride precursors shows the maximum area under the curve, whereas for electrode (B) and (C) obtained from nitrate and acetate precursors shows decrease in redox peaks and less area under curve. The calculated maximum value of specific capacitance for electrode (A) was 237.68 F/g, 102.03 F/g for electrode (B) and 59.91 F/g for electrode (C). Figure 7 (b) represents the CV's of cobalt oxide electrode prepared using different solution concentration variation for optimized ingredient cobalt chloride (A). CV's of all the electrodes were carried out at scan rate 5 mV/s in 1 M KOH within the potential window - 0.92 to 0.45 V. From the CV curve it is clearly observed that sample M_2 shows maximum area under the curve and with large redox peaks, electrode M_1 to M_6 shows decrease in area under curve and redox peaks. The *SC* associated with the electrode was calculated for various electrodes. The maximum *SC* value 237.68 F/g was obtained for electrode M_2. Corresponding *SC* values are 204.91 F/g, 237.68 F/g, 157.82 F/g, 118.58 F/g, 95.62 F/g and 87.64 F/g for M_1, M_2, M_3, M_4, M_5 and M_6, respectively. The redox peaks may occur due to the charge transfer process between electrode and electrolyte. Extraction of ions and electrons from the film is associated with the oxidation peaks, whereas

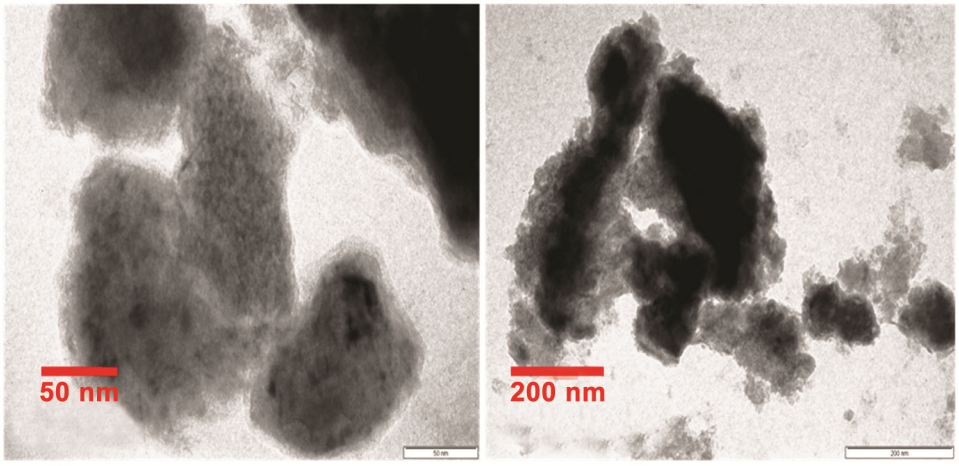

Fig. 6 — TEM image of D_2 sample.

insertion of ions and electrons into the film is associated with the reduction peaks[43].

Figure 7 (c) shows CVs of typical electrodes D_2, D_3 and D_5 carried out at the scan rate 5 mV/s in 1 M KOH in potential range - 0.92 to 0.45 V. All CV shows

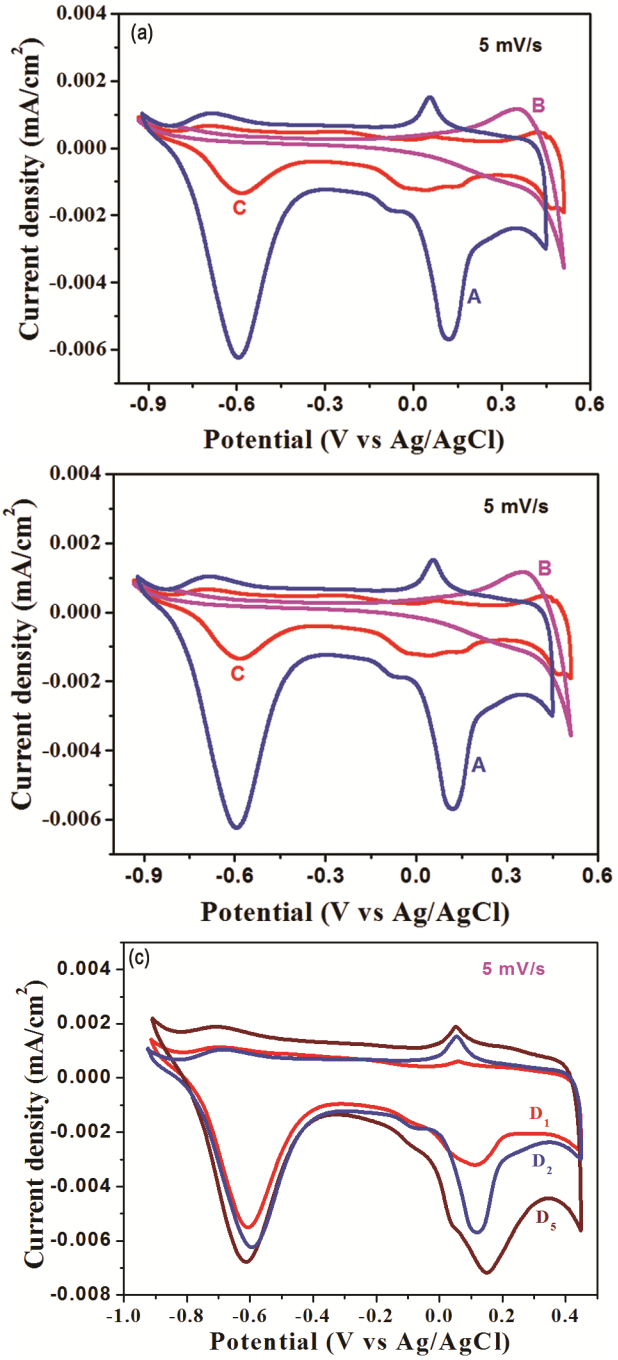

Fig.7 — (a) Cyclic voltammogram of electrodes A, B and C carried at scan rate 5 mV/s in 1MKOH, (b) cyclic voltammogram of electrode M_1, M_2, M_3, M_4, M_5 and M_6 carried at 5 mV/sec in 1 M KOH and (c) cyclic voltammogram of electrode D_2, D_3 and D_5 carried at 5 mV/s in 1 M KOH.

mixed-capacitive nature with redox peaks at the respective anodic and cathodic sweeps. It can be observed from the CV that D_5 electrode shows large area under curve, current density, electrode D_2 shows less area under curve compared to D_5 and D_1 shows less area under curve and current density. The calculated value of SC for D_1 electrode was 177.83 F/g, $D_2$is 237.68 F/g and D_5 is 159.95 F/g. Electrode D_2 shows maximum value of SC as compared to other electrodes. This may be attributed to the uniform growth of granular type of morphology of the film as compared to other films. However, though the sample D_5 shows larger current density, weight of the deposited active material is much larger due to longer deposition time interval which effect on the electrochemical performance of the D_5.

3.6.2 Chronopotentiometry

Figure 8 shows charge-discharge behavior of M_2 electrode scanned in 1 M KOH for different current densities like 5, 10, 15, 25 and 40 mA/cm^2. Here it was observed that with increase in current density, charge discharge curves shifts towards symmetric nature. In point of fact at 15 mA/cm^2 current density, electrode shows nearly symmetric charge-discharge behaviour as compared to others which indicates nearly rectangular nature of the CV curve (*i.e.*, ideal behaviour). The linear decrease in the potential drop (ohmic drop) observed at lower current density itself indicates the pseudocapacitive behavior of the prepared electrode. The electrical parameter such as SE, SP and η were calculated from charge-discharge curves using the relations (3) to (5).The calculated value of SE, SP and η are given in Table 1. The highest calculated values of SE, SP and η were 4.91Wh/kg and 28.69 kW/kg and 94.78 %, respectively.

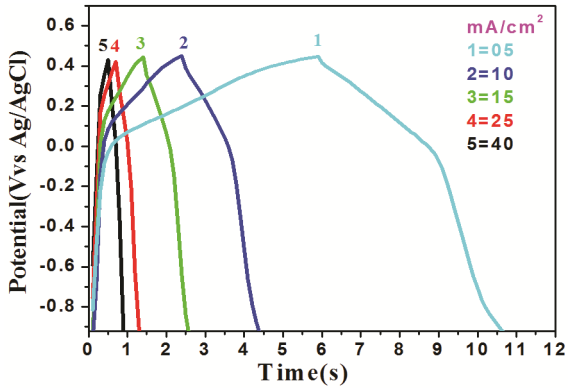

Fig. 8 — Charge-discharge curve of D_2 electrode carried at different current densities (mA/cm^2).

Table 1 — SE, SP and η for the optimized electrode D_2.

Current density (mA/cm^2)	Specific energy (Wh/kg)	Specific power (kW/kg)	Efficiency (%)
5	4.91	3.58	66.82
10	3.94	7.17	68.32
15	3.14	10.75	65.47
20	3.14	14.34	87.6
25	2.99	17.93	86.84
30	3.00	21.51	83.20
35	2.82	25.10	80.99
40	3.15	28.69	94.78

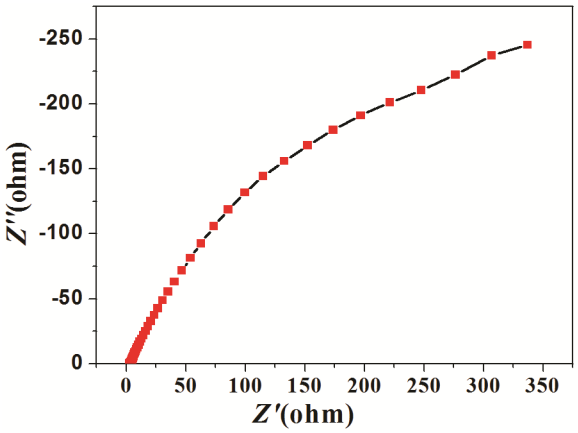

Fig. 9 — Nyquist plot of D_2 electrode.

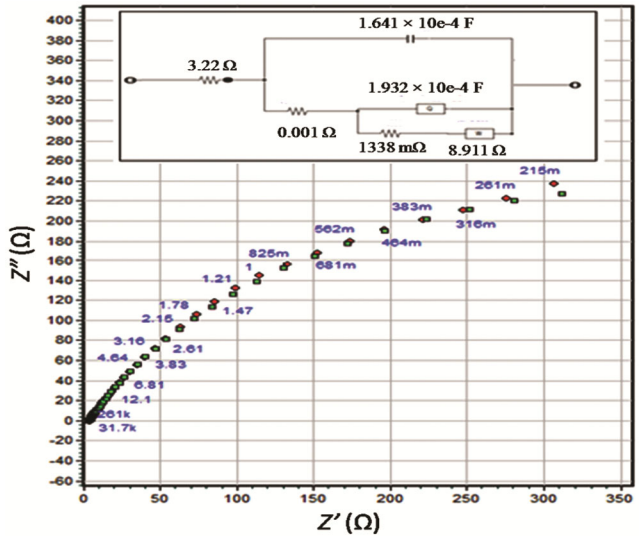

Fig. 10 — Matched Nyquist plot of D_2 electrode.

3.6.3 Electrochemical impedance spectroscopy

Using electrochemical impedance spectroscopy (EIS) technique, internal resistance and capacitive behavior of D_2 electrode was studied at operating open circuit potential (OCP) - 0.38 V in 1 M KOH in the frequency range of 1 mHz to 1 MHz. Figure 9 shows the Nyquist plot of (Z″ vs Z′) imaginary and real impedance. Nyquist plot composed of three regions, at higher frequency region a depressed semicircle results from a parallel combination of the charge-transfer resistance (R_{ct}) caused by the faradaic reactions at the lower frequency region. The observed internal resistance (R_i) was around 3.56 Ω. Portion of the curve having an inclination of ~ 45° with imaginary axis gives the value of warburg resistance (W) and is related to the frequency dependent diffusion resistance of electrolyte ions resulted at the time of intercalation in pores of electrode. Figure 10 (Nyquist plot of Z″ versus Z′) shows the experimental and standard curves obtained by simulation using ZsimpWin software of Co_3O_4 electrode and inset of it shows matched equivalent circuit. The observed circuitry parameters are capacitance C_1= 1.641×10^{-4} F, pseudocapacitance Q = 1.932×10^{-4} F, R_1 =3.22 Ω, R_2 =0.001 Ω and R_3 =1338 mΩ and Warburg resistance W = 8.911 Ω, respectively.

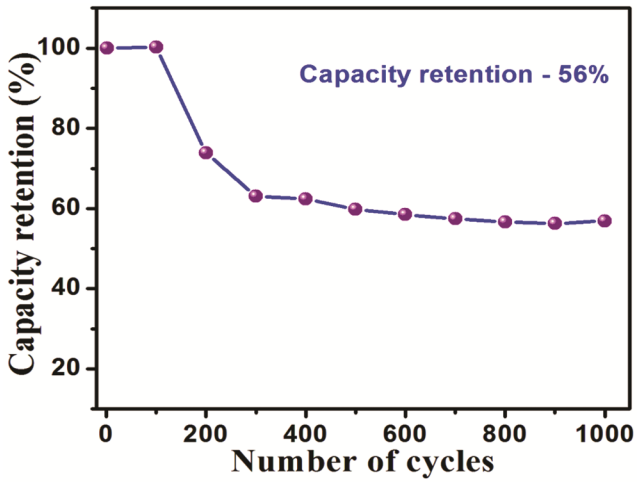

Fig. 11 — Stability curve of D_2 electrode carried at 100 mV/s.

3.6.4 Stability

To know the durability of the prepared electrode, stability test was carried out at the scan rate of 100 mV/s in 1 M KOH up to 1000 cycles. Figure 11 shows stability test curve of D_2 electrode, which shows a stable value of *SC* after 500 cycles. The decrease in % capacitance was found to be 59%. This may be attributed to the degradation of active material for large cycle numbers within the electrolyte bath during the potential cycling at higher scan rate.

4 Conclusions

Co_3O_4 electrodes were prepared successfully by template-free binder-less potentiodynamic electrodeposition technique. All the prepared samples

were characterized by XRD shows polycrystalline cubic face centered crystal structure. Different precursors give agglomerated grains, randomly distributed nanoflakes and interconnected nanoflakes like morphology confirmed by FE-SEM and TEM images. Solution concentration and deposition time optimization enhances morphology and the electrochemical performance. Electrochemical CV characterization indicates pseudocapacitive behavior. The maximum value of *SC* in 1 M KOH was 237.38 F/g. The obtained specific energy, specific power and columbic efficiency for the optimized electrode (0.1 M deposited for 30 min) were 4.91 Wh/kg, 28.69 kW/kg and 94.78%, respectively. EIS of complex impedance spectra shows internal resistance of 3.55 Ω.

Acknowledgment

One of the authors Dr B J Lokhande is grateful to thanks Bhabha Atomic Research Center (BARC), Mumbai and DST-SERB, New Delhi for providing financial support through the project scheme 2010/34/46/BRNS/2228 and DST.

References

1 Li Z, Luo W, Zhang M, Feng J & Zou Z, *Energy Environ Sci*, 6 (2013) 347.
2 Qorbani M, Naseri, N, Moradlou O, Azimirad R & Moshfegh A Z, *Appl Catal B*, 162 (2015) 210.
3 Atwater H A & Polman A, *Nat Mater*, 9 (2010) 205.
4 Xiao Z, Bi C, Shao Y, Dong Q, Wang Q, Yuan Y, Wang C, Gao Y & Huang J, *Energy Environ Sci*, 7 (2014) 2619.
5 Hu W, Yu G, Pan L, Liu N, McDowell M T, Bao Z & Cui Y, *Nat Commun*, 4 (2013) 1943.
6 Zinth V, von Lüders C, Hofmann M, Hattendorff J, Buchberger I, Erhard S & Gilles R, *J Power Sources*, 271 (2014) 152.
7 GaoY, Chen S, Cao D, Wang G & Yin J, *J Power Sources*, 195 (2010) 1757.
8 Kötz R & Carlen M, *Electrochim Acta*, 45 (2000) 2483.
9 Wei W, Cui X, Chen W & Ivey D G, *Chem Soc Rev*, 40 (2011) 1697.
10 Yang Q, Lu Z, Sun X & Liu J, *Sci Rep*, 3 (2013) 3537.
11 Hercule K M, Wei Q, Khan A M, Zhao Y, Tian X & Mai L, *Nano Lett*, 13(2013) 5685.
12 Ryu I,Yang M, Kwon H, Park H K, Do Y R, Lee S B & Yim S, *Langmuir*, 30 (2014) 1704.
13 Li Q, Wang Z L, Li G R, Guo R, Ding L X & Tang Y X, *Nano Lett*, 12 (2012) 3803.
14 Liu Y, Yan D, Li Y, Wu Z, Zhuo R, Li S, Feng J, Wang J, Yan P & Geng Z, *Electrochim Acta*, 117 (2014) 528.
15 Xiong G, Hembram K P S S, Reifenberger R G & Fisher T S, *J Power Sources*, 227 (2013) 254.
16 Yuan C, Yang L, Hou L, Shen L, Zhang X & Lou X D, *Energy Environ Sci*, 5 (2012) 7883.
17 Rakhi R B, Chen W, Hedhili M N, Cha D & Alshareef H N, *ACS Appl Mater*, 6 (2014) 4196.
18 Xue T & Lee J, *J Power Sources*, 245 (2014) 194.
19 Dam D T, Wang X & Lee J, *ACS Appl Mater Interfaces*, 6 (2014) 20729.
20 Kore R M, Mane R S, Naushad M, Khan M R & Lokhande B J, *RSC Adv*, 6 (2016) 24478.
21 Wang D, Li F & Cheng H M, *J Power Sources*, 185 (2008) 1563.
22 Ma X, Li Y, Wen Z, Gao F, Liang C & Che R, *Appl Mater Interfaces*, 7 (2014) 974.
23 Lokhande B J, Ambare R C, Mane R S & Bharadwaj S R, *Curr Appl Phys*, 13(2013) 985.
24 Chen Z, Chen Y, Zuo C, Zhou S, Xiao AG & Pan A X, *Bull Mater Sci*, 36 (2013) 239.
25 Wang H, Qing C, Guo J, Aref A A, Sun D,Wang B & Tang Y, *J Mater Chem A*, 2 (2014) 11776.
26 Xia X, Tu J, Zhang Y, Mai Y, Wang X, Gu C & Zhao X, *RSC Adv*, 2 (2012) 1835.
27 Yuan C, Yang L, Hou L, Shen L, Zhang F, Li D & Zhang X, *J Mater Chem*, 21(2011) 18183.
28 Xia X H, Tu J, Mai Y, Wang X, Gu C & Zhao X, *J Mater Chem*, 21 (2011) 9319.
29 Gao Y Y, Chen S L, Cao D X, Wang G L & Yin J L, *J Power Sources*, 195 (2010) 1757.
30 Xu J, Gao L, Cao J, Wang W & Chen Z, *Electrochim Acta*, 56 (2010) 732.
31 Fan Y, Shao H, Wang J, Liu L, Zhang J & Cao C, *Chem Commun*, 47 (2011) 3469.
32 Jagadale A D, Dubal D P & Lokhande C D, *Mater Res Bull*, 47 (2012) 672.
33 Thornton J A, *Sci Technol A*, 4 (1986) 3059.
34 Kitarnoto Y, Zhang M, Haijima S, Matsumoto K & Abe M, *J Phys IV France*, 7 (1997) 581.
35 Wang G L, Wang W, Zhao Y F, Shao G J & Liu T T, *Ionics*, 20 (2014) 243.
36 Gujar T P, Shinde V R, Lokhande C D, Mane R S & Han S H, *Appl Surf Sci*, 250 (2005) 161.
37 Kandalkar S G, Lokhande C D, Mane R S & Han S H, *Appl Surf Sci*, 253 (2007) 3952.
38 Jagadale A D, Guan G, Li X, Du X, Ma X, Hao X & Abudula A, *J Power Sources*, 306 (2016) 526.
39 Sharma B K, *Electrochemistry*, 5th Edn, (Goel publishing house), (1997) 153.
40 Feng J J, Li A Q, Wang A J, Lei Z & Chen J R, *Microchim Acta*, 173 (2011) 383.
41 Bockman O, Ostvold T, Voyiatzis G A & Papatheodorou G N, *Hydrometallurgy*, 55 (2000) 93.
42 Koza J A, Zhen H, Miller A S & Switzer J A, *Chem Mater*, 24 (2012) 3567.
43 Xia X H,Tu J P, Zang J, Huang X H, Wang X L, Zhang W K & Huang H, *Electrochem Commun*, 10 (2008) 1815.